Fatigue of Aircraft Structures
Vol.1 (2012) 123-140
10.2478/v10164-012-0064-3

THE MMM EXPERT SYSTEM: FROM A REFERENCE SIGNAL TO THE METHOD VALIDATION

Mirosław Witoś

Air Force Institute of Technology, Warsaw, Poland

Abstract

This paper presents the first step in the methodological approach to the validation of the metal magnetic memory (MMM) method in the non-destructive testing (NDT) applications and in the systems used for diagnosis of early stages of material fatigue in mechanical constructions (structural health monitoring, SHM, and prognosis health management, PHM). The study is focused on the properties of the external natural source of magnetisation of the object under MMM examination and the impact of the magnetisation components. The precise data obtained from measurements of the Earth's geomagnetism (from ground stations and satellites) and the revised model of the Earth's magnetism can be applied in order to calibrate high sensitivity magnetic field sensors, validate the measurement results and extend the functional capacity of the MMM method.

Keywords: geomagnetic field, magneto-mechanical effects, numerical model, SHM

1. INTRODUCTION

Magneto-mechanical effects (MME) are increasingly used to diagnose critical structural elements that are made of ferromagnetic and paramagnetic materials. In non-destructive testing (NDT) and systems to monitor early fatigue symptoms (structural health monitoring, SHM, prognosis health management, PHM), the following processes are used [1-5]:

- reversible paraprocesses (Joule'a effect, Villari effect and derivative phenomena),
- irreversible paraprocesses (ΔE effect, Metal Magnetic Memory (MMM), which is an equivalent of Natural Remanent Magnetization (NRM) in geophysics).

Diagnostic information not only about the level of the dislocation concentration (1st phase of fatigue) and cracks but also about changes in internal stresses and the history of maximal material effort can be obtained by means of non contact measuring of the magnetization level and distribution, Fig. 1. These features are the base for the Metal Magnetic Memory method [6-12].

The interpretation of the results to be used in the MMM method (research without artificial magnetization of metal) is difficult. The main problems are as follows:

- **natural magnetization signal** – the Earth's magnetic field is weak, its intensity and components are dependant on a place and time of performed research;
- **magnetization of the polycrystalline structure with different defects** – shortage of systematized knowledge on magnetic features of constructional steel, simplified models of magnetization without periodical components and noise of the Earth's magnetic field;
- **reference signal** – differential measurements applied in geophysical research and some MMM applications, Fig. 2. (increasing sensitivity of measurements) may not be applicable in the interiors with strong ferromagnetic objects (i.e. a palisade of the compressor/turbine blade).

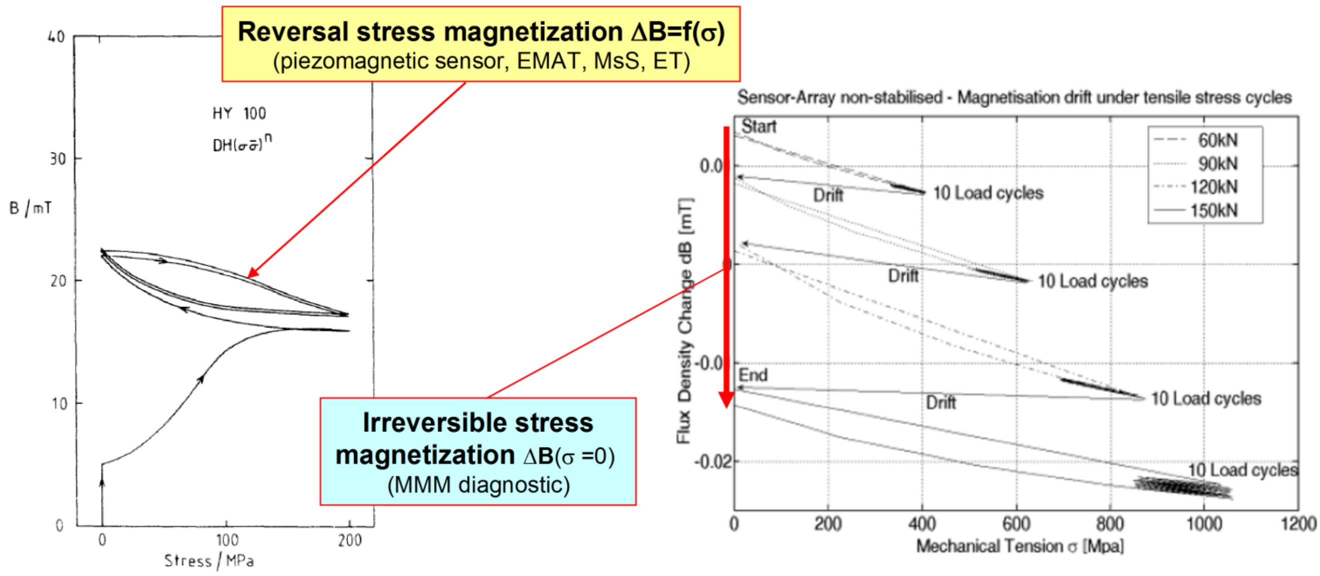

a)

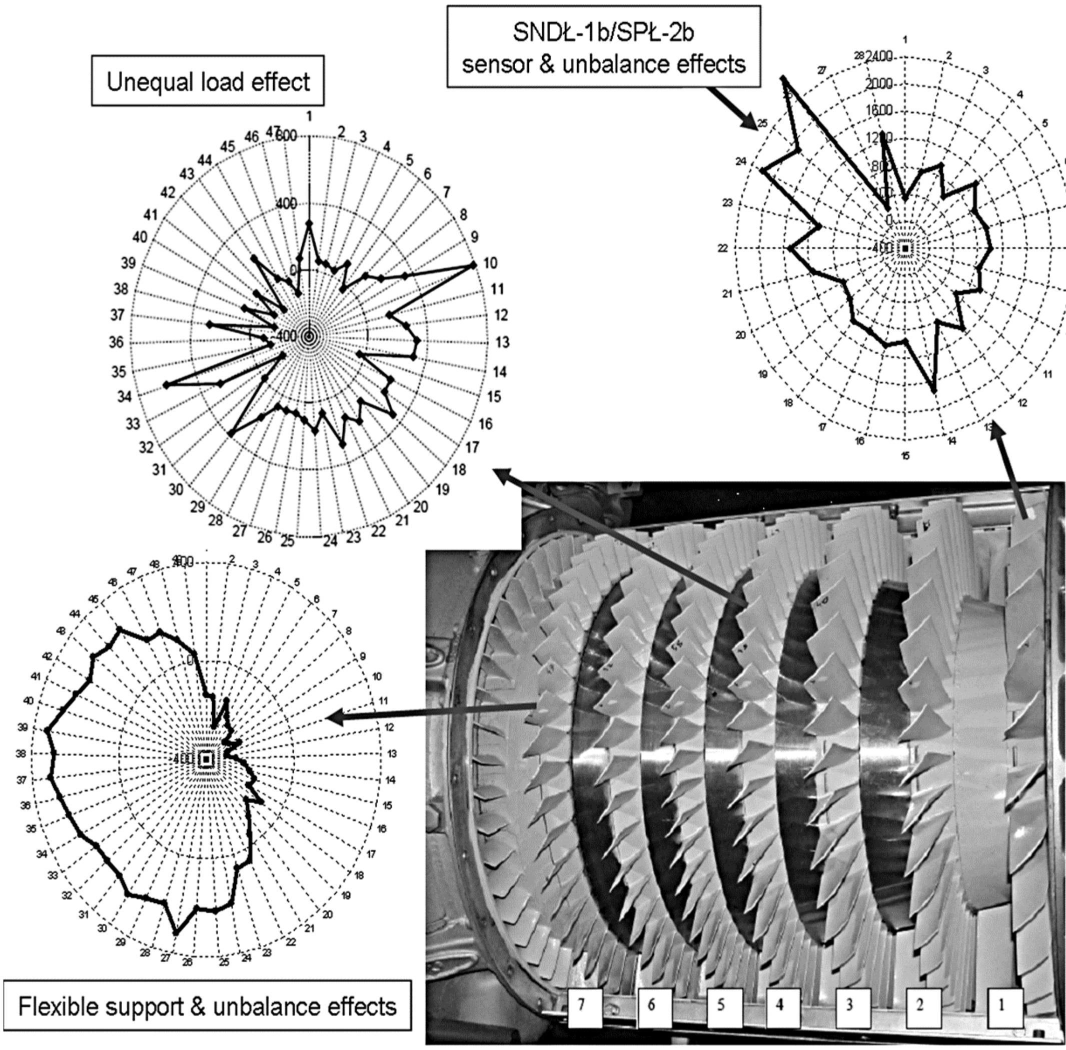

b)

***Fig. 1. Detection of stress prehistory: a) reversible and irreversible process of stress magnetization* [3]*; b) identification of blade fatigue risk (H_p =f(blade number))* [5]**

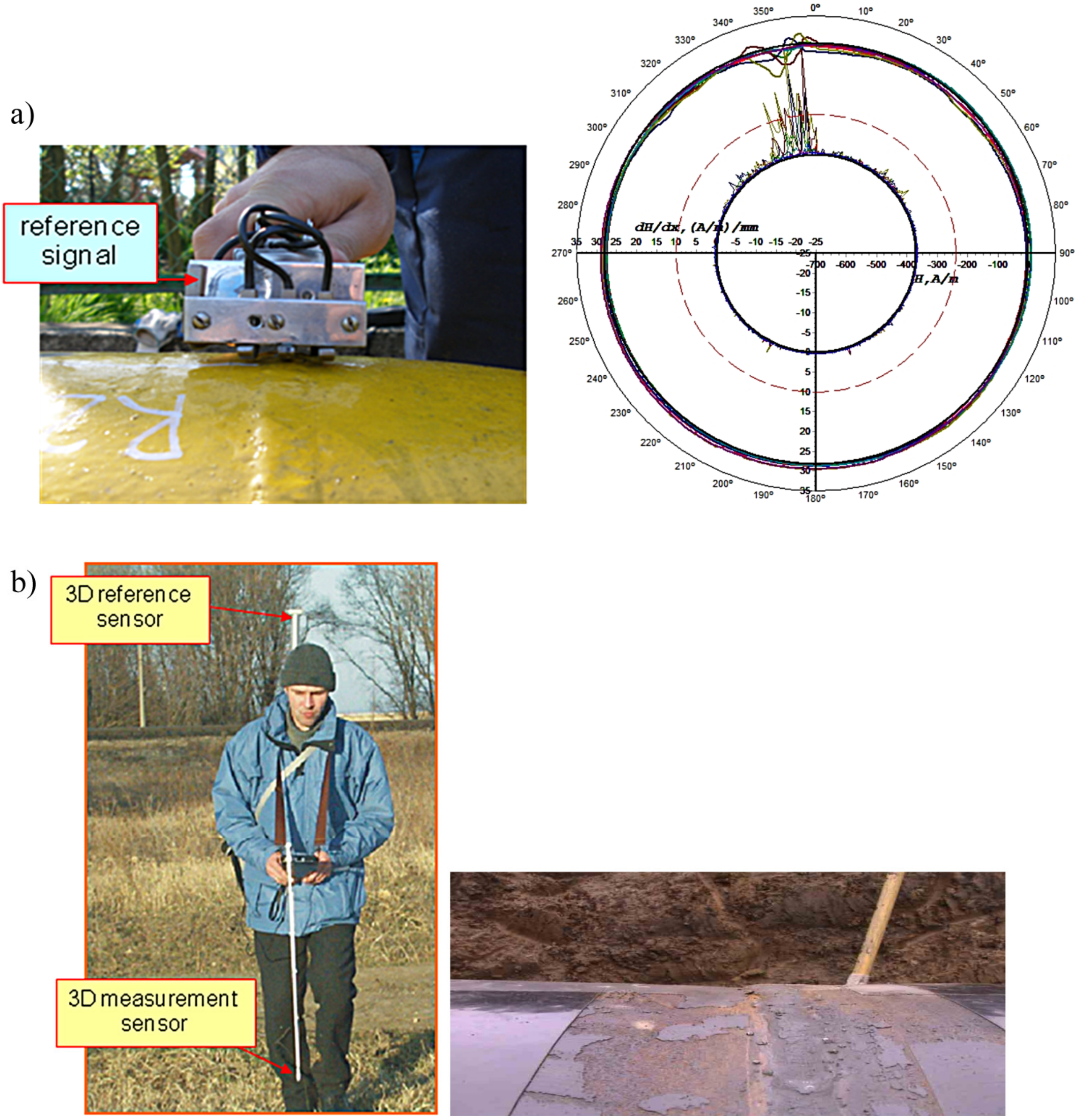

Fig. 2. MPM sensors of Energodiagnostika Ltd company: a) multichannel 2D gradient sensor for welds testing according to PN-ISO 24497:1-3 (2009) with resolution dH = ±2.0 A/m; b) 3D gradient sensor for NDT of underground pipes with resolution dH = ±0.02 A/m

This paper presents a proposal to support the MMM method by means of data from numerical models of the Earth's magnetism, the INTERMAGNET database and the NOAA/SWPC space alerts.

2. THE THEORY OF THE MMM METHOD

When a substance is exposed to the influence of a magnetic field, it behaves in various ways, depending upon the physical and chemical properties of the material examined. Each substance, be it a gas, a liquid, or a solid, exhibits its own peculiar characteristics when magnetized, Fig. 3.

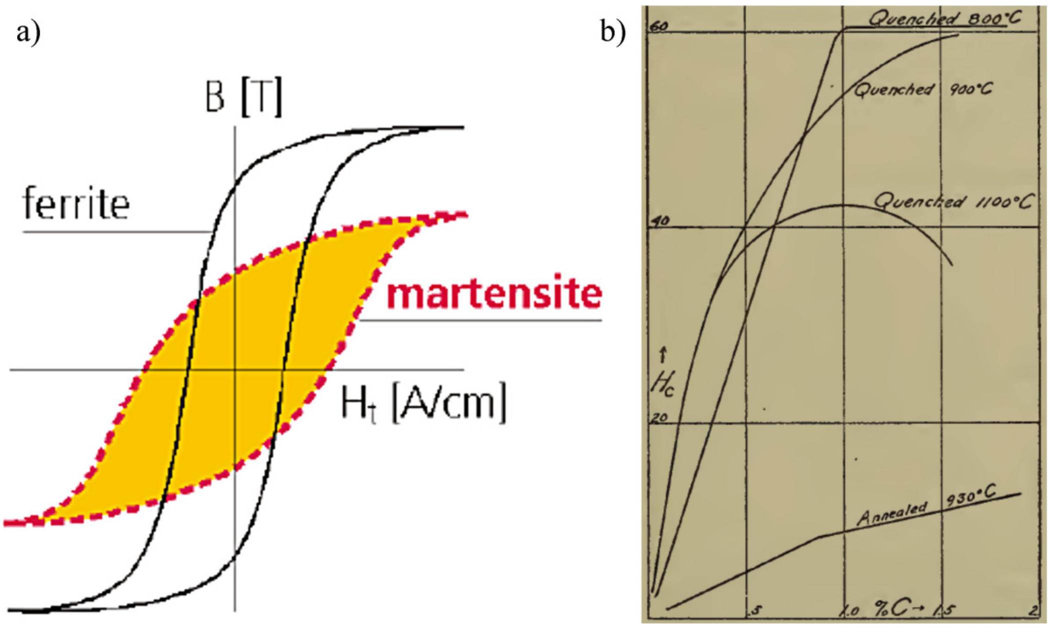

***Fig. 3. a) difference between the shape of a hysteretic loop B-H for ferrite and martensite steel* [13]; *b) the variation of coercive force with carbon content for different heat treatments (CGS units)* [14]**

The constitutive law that relates material magnetization **M** to magnetic field **H** and magnetic induction **B** is described by the equation (1)

$$\mathbf{B} = \mu\mathbf{H} = \underset{SI\ system\ of\ units}{\mu_0(\mathbf{H} + \mathbf{M})} = \underset{CGS\ system\ of\ units}{\mathbf{H} + 4\pi\mathbf{M}}$$

$$\mathbf{M} = \frac{1}{V}\sum_V \mathbf{m} \tag{1}$$

$$\mathbf{m} = f(\rho_a, \mu_a, K_1, K_2, T, \sigma_I, \sigma_{II}, \sigma_{III}, H) = f(\lambda, \omega, E, v)$$

where μ and μ_0 denote the permeability of the substance and vacuum (SI unit constant, $\mu_0 = 4\pi\ 10^{-7}$ H/m); V is the substance volume; **m** is the magnetization of the elementary molecules (the net magnetic moment), which is the result of an orbital magnetic moment associated with the electron orbital angular momentum, and a spin magnetic moment associated with the electron spin. The symbols ρ_a and μ_a denote atomic density and atomic magnetic moment, respectively. These depend on the chemical composition of material and the elementary unit cell of lattice. The symbols K_1 and K_2 denote structural anisotropy constants of crystal (elementary unit cell of lattice). The symbol T denotes material temperature. The symbols σ_I, σ_{II} and σ_{III} denote the residual and applied stresses. Long–range stresses (type I) equilibrate over macroscopic dimensions. Type II stresses equilibrates over a number of grain dimensions. Type III stresses on the other hand exist over atomic dimensions and balance within the grain. The symbol λ and ω denotes two components of magnetostriction (the fraction change of length $\lambda = \frac{\Delta l}{l}$ and volume $\omega = \frac{\Delta V}{V}$ exhibited by a substance when exposed to a magnetic field). The symbol E and ν denote the Young modulus and the Poisson coefficient.

The actual magnetization state of the material can be described with the following formula:

$$\mathbf{M}(H, T, \sigma) = (1 + k_H)\cdot(1 + k_T)\cdot(1 + k_\sigma)\cdot\mathbf{M}_0 \tag{2}$$

in which k_H, k_T, k_σ are the nonlinear coefficients of the external magnetic field influence **H**, material temperature T and stress tensor σ on the change of initial magnetization $\mathbf{M}_0$ of the material.

The material's reaction to external excitation/loads can be characterized by a linear approximation with the use of the tensor relations (3a-3d) [15-17], in which temperature T, stress σ, electric current I and magnetic intensity H serve as independent variables. Entropy S which shows the direction of change, strain ε, electric displacement field D and magnetic field B are the dependent variables.

$$dS = \alpha_{ij}^{HI}\sigma_{ij} + i_n^{I\sigma}H_n + p_m^{H\sigma}I_m + \frac{\rho C^{HI\sigma}}{T}dT \tag{3a}$$

$$\varepsilon_{ij} = s_{ijkl}^{HIT}\sigma_{kl} + d_{ijn}^{IT}H_n + d_{ijm}^{HT}I_m + \alpha_{ij}^{HI}\Delta T \tag{3b}$$

$$B_m = d_{mij}^{IT}\sigma_{ij} + \mu_{mn}^{IT\sigma}H_n + m_{mn}^{T\sigma}E_n + i_m^{I\sigma}dT \tag{3c}$$

$$D_m = d_{mij}^{HT}\sigma_{ij} + m_{mn}^{T\sigma}H_n + \gamma_{mn}^{HT\sigma}I_m + p_m^{H\sigma}dT \tag{3d}$$

The subscripts $i, j, ..., n = 1, 2, 3$ are address pointers of the tensor, whereas the superscripts describe the independent variables that have influence on the 11 coefficients representing material data: elasticity s, density ρ, thermal expansion α, heat capacity C, dielectric permittivity γ, magnetoelectricity m, piezoelectric d^{HT}, pizoelectricity p, magnetic permeability μ, piezomagneticity d^{IT}, and piromagneticity i. Values of these coefficients are determined for constant values of independent variables.

For a specified temperature, MME is described by the nonlinear tensor relations:

$$\varepsilon_{ij} = s_{ijkl}^{HT}\sigma_{kl} + d_{ijn}H_n \tag{4a}$$

$$B_m = d_{mij}^{*}\sigma_{ij} + \mu_{mn}^{T\sigma}H_n \tag{4b}$$

in which $d = \left.\frac{\partial \varepsilon}{\partial H}\right|_{\sigma}$ and $d^* = \left.\frac{\partial B}{\partial \sigma}\right|_{H}$ are the magneto-mechanical coefficients obtained experimentally for each material with stresses and the magnetic field held constant.

The formula (4a) models the generalized Joule effect. Total material strain ε is a resultant of mechanical ε_{mech} and magnetic ε_{mag} strain (linear λ and volumetric ω magnetostriction) [18-23].

$$\varepsilon = \varepsilon_{mech} + \varepsilon_{mag} \tag{5}$$

Formula (4b) models the generalized Villari effect – magnetic field generation by a ferromagnetic object has a mechanical component B_{mech} (piezomagnetism) and a magnetic component B_{mag} (material's reaction to an external magnetic field).

$$B = B_{mech} + B_{mag} \tag{6}$$

In a weak magnetic field the amplitude of magnetic induction $|B_{mech}| >> |B_{mag}|$ for moderate to high levels of material elastic strain. The stress-magnetization curve B(σ) from Fig. 4:

- depends on external magnetic intensity **H**,
- has an extremum (kink) below the plastic limit $R_{e0.2}$.

a) b)

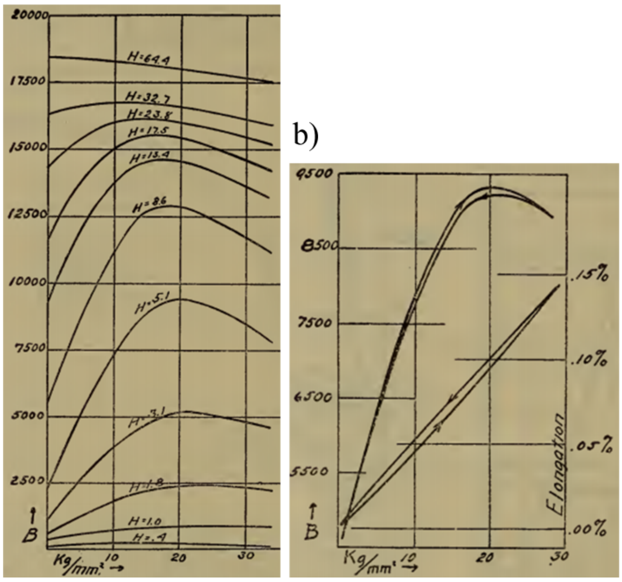

***Fig. 4. Showing: a) the effect of tension on the magnetization under different field strengths; b) hysteresis in the magnetic and the mechanical properties of a steel under a changing tensile force whose maximum exceeds the elastic limits* [14]**

A ferromagnetic object contains information about its technical condition and loading history in its magnetization change. Nonlinear magnetic properties of a ferromagnetic material enable **the memorization of load history**, which can be read by examining the change in the magnetization distribution/map after the examined element is unloaded (first load cycle effect), Fig 5.a). Stress magnetization of a material in the weak and constant Earth's magnetic field is different from technological magnetization with a strong field. The hysteresis loop for stress magnetization is repeatable only after 10-15 load cycles [3].

a) b) c)

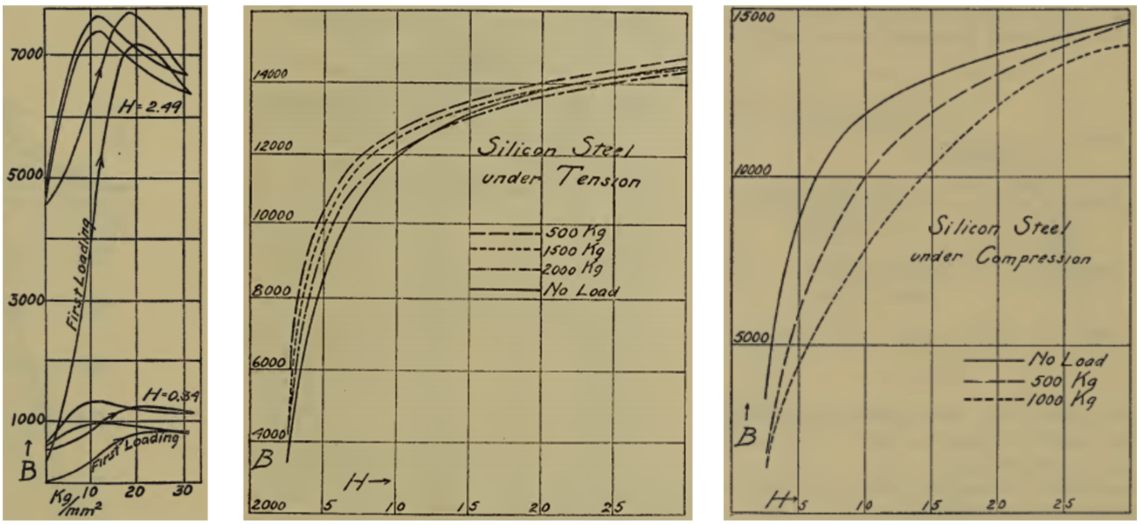

Fig. 5. a) changes in magnetic induction due to the loading and unloading of a bar under constant magnetizing force* [14]*; b) and c) magnetic changes due to tension and compression for stresses below the elastic limit* [24] *(CGS units)

Tension of non-alloy steel in the elastic strain regime increases the magnetic induction in the direction of the load applied, Fig 5.b). In the direction transverse to the loading (one in which compression occurs) the trend of change in induction is opposite, Fig. 5.c). The permeability and magnetostriction have been also changed, Fig. 6. For stresses greater than the elastic limit it is evident that both the contour and magnitudes of the curves are changed, Fig. 7.a). The manner in which the magnetic flux decreases during the elongation of the shows Fig. 7.b). The decrease in flux is not proportional to the elongation, so that it is evident that there is some change other than a decrease in the cross section taking place within the bar. The greater part of this structural change takes place during the initial elongations. The true elastic limit is easily determined by this magnetic method, Fig 7.c), and corresponds to a critical point of molecular equilibrium. The apparent elastic limit or yield point is a function of the previous working of the metal, and, consequently, does not characterize the metal. The nature of the material is best indicated by the specific plastic load [14].

a)

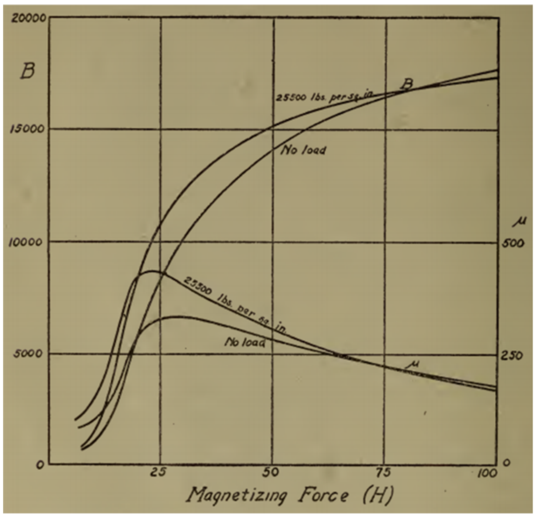

b)

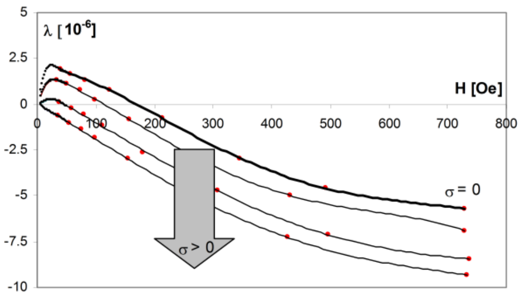

Fig. 6. a) the effect of a relatively moderate degree of tension on the magnetic permeability of steel wire* [25]*; b) influence of tension on magnetostriction of iron* [20] *(CGS units)

a) b)

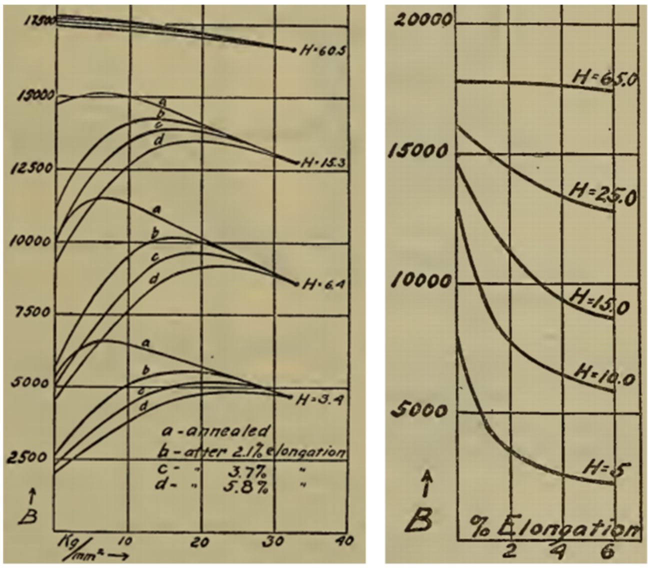

c)

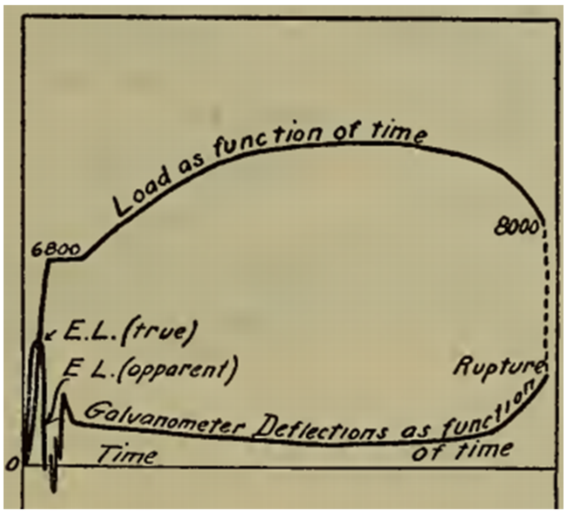

Fig. 7. a) the way in which the effect of tension on the magnetic properties is modified by cold working; b) the decrease in magnetic induction corresponding to a given magnetizing force when the test specimen is stretched beyond the elastic limit; c) the changes in tension and in the magnetic properties when the tensile machine motor is driven uniformly* [14] *(CGS units)

Local structural "defects" which can be observed in the changes of magnetic permeability are a source of magnetic anomalies (deviation from the anticipated trend that takes into account the demagnetization tensor). The above conclusions provide a theoretical background for all the magnetic NDT methods (both active and passive) [26-28].

2.1. The diagnostic signal in the Metal Magnetic Memory method

The MMM method uses the impact of the weak magnetic field of the Earth $\boldsymbol{B}_m$ and electromagnetic noise $\boldsymbol{\varepsilon}_m$ (of the external natural magnetic field $\boldsymbol{B}_e$) to observe the changes in the local magnetic, electric and mechanical properties of the polycrystalline material (mapped among others by orthogonal components of the magnetic permeability $\boldsymbol{\mu} = \lfloor \mu_{\|}, \mu_{\perp}, \mu_n \rfloor$, electric conductivity $\boldsymbol{\rho} = \lfloor \rho_{\|}, \rho_{\perp}, \rho_n \rfloor$ and Young's modulus $\mathbf{E} = [E_{II}, E_{\perp}, E_n]$ of the component under examination) – transmittance $\mathbf{G}$. The value to measure is the magnetic field $\mathbf{B}_p$ close to the monitoring object, Fig. 8, whose value results from the local structural and magnetic anisotropy of the material $\mathbf{S}$ **(**magnetization $\mathbf{M}$**)** and distance $\Delta\mathbf{r}$ between the object and magnetic sensor.

The health of the object and the fatigue stage of its material (mapped by mechanical and physical local properties) are expressed by the relation:

$$\mathbf{B}_p(\mathbf{S}, \mathbf{M}, \mathbf{r} + \Delta\mathbf{r}, t) = \mathbf{B}_e(\mathbf{r}, t) \cdot \mathbf{G}(\boldsymbol{\mu}, \boldsymbol{\rho}, \mathbf{E}, \Delta\mathbf{r}, t) = (\mathbf{B}_m(\mathbf{r}, t) + \boldsymbol{\varepsilon}_m(\mathbf{r}, t)) \cdot \mathbf{G}(\boldsymbol{\mu}, \boldsymbol{\rho}, \mathbf{E}, \Delta\mathbf{r}, t)$$
$$\mathbf{B}_p \propto \mathbf{U} = -\int_v \mathbf{M} \, grad \frac{1}{\Delta r} \, dv \tag{7}$$

where: t – measurement time, $\mathbf{r}$ – coordinates of the measuring point ($\mathbf{r} = (\lambda, \varphi, r)$ in global geocentric (field)/geographical (object) coordinates or $\mathbf{r} = (x, y, z)$ in local Cartesian coordinates (object/sensor), $r = a + h$ (a = 6371200 m – the Earth's radius, h – WGS-84 ellipsoid altitude), $\boldsymbol{\mu}$, $\boldsymbol{\rho}$, $\mathbf{E}$ – magnetic, electric and mechanical properties of the polycrystalline material, $\Delta r < 5$ m, $\mathbf{U}$ – magnetic potential at a measurement point.

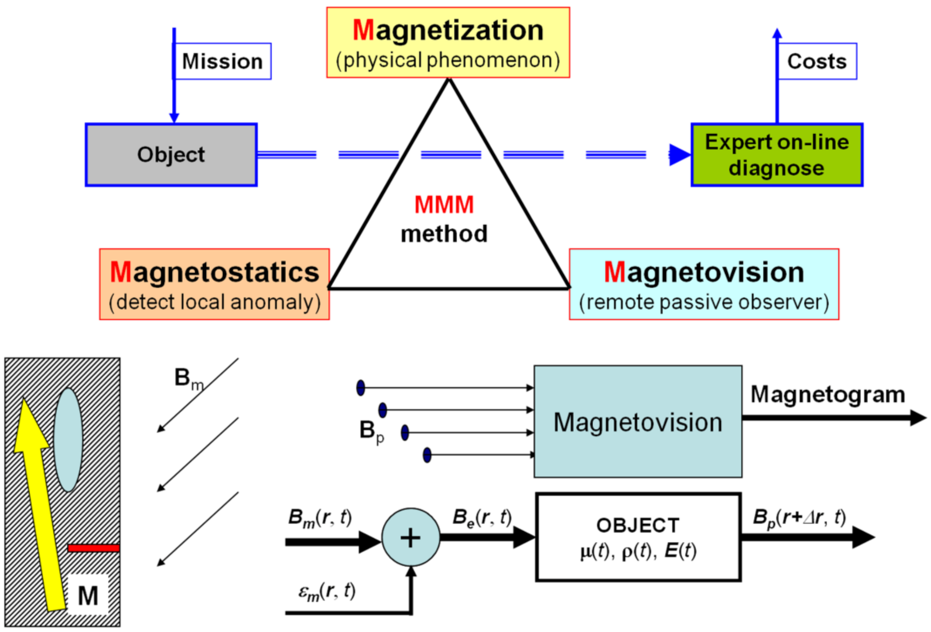

Fig. 8. The concept of MMM testing. Small structural defects (cracks, inclusions) are local sort-wave magnetic anomalies. Local plasticity (pinning domain) is a medium-wave magnetic anomaly. Stress and volume damage of structure change the average magnetic properties of a body and the trend of magnetization.

Material variables **μ**, **ρ, E** (scalar tensors) depend among others on the type (grade) and structure of the material, the external magnetic field intensity, applied and residual stresses, material temperature, dislocation density (manufacture quality and events health) and external excitation (level, frequency and historic). Material variables are complex data that describe nonlinear property of the material. The real parts of μ, ρ, **E** describe reversible sub-processes (i.e. Villary effect); the imaginary parts describe irreversible sub-processes (losses) present during the electric current flow, technical and stress magnetization (stress-strain cycles) and structure damage (residual stress redistribution, LCF, HCF, VHCF and TMF fatigue). Micro- or macro- plastic deformation affects the hysteretic magnetic properties of steels because it changes the dislocation density, which affects domain-wall movement and pinning, and also because it places the specimen under residual strain.

Current material properties **G** are defined as:

$$\mathbf{G}(\boldsymbol{\mu},\boldsymbol{\rho},\mathbf{E},\Delta\mathbf{r},t)=\frac{\mathbf{B}_p(\mathbf{S},\mathbf{M},\mathbf{r}+\Delta\mathbf{r},t)}{\mathbf{B}_m(\mathbf{r},t)+\boldsymbol{\varepsilon}_m(\mathbf{r},t)}\cong 1+\frac{\Delta\mathbf{B}(\mathbf{S},\mathbf{M},\mathbf{r}+\Delta\mathbf{r},t)}{\mathbf{B}_{m\_ref}(\mathbf{r},t)} \tag{8}$$

In order to obtain, by means of the MMM method, a reliable identification of the material health based on the signal $\mathbf{B}_p$, it is essential to know the magnetic properties of the Earth's magnetic field $\mathbf{B}_m$ and electromagnetic noise $\boldsymbol{\varepsilon}_m$. For NDT, SHM and PHM applications, the reference signal $\mathbf{B}_{m\_ref}$ will be used [29].

3. THE EARTH'S MAGNETIC FIELD

The Earth is like a giant magnet. At every location on or above the Earth, its magnetic field has a more or less well-known direction, which can be used not only as a reference frame to orient ships, aircraft and handheld devices but also as a reference signal for NDT, SHM and PHM applications. The magnetic field $\mathbf{B}_m$ at or near the surface of the Earth is a combination of the Earth's magnetic field and fields of external (solar, space) origin [30-33]. The geomagnetic field is a sum of contributions:

$$\mathbf{B}_m(\mathbf{r},t)=\underbrace{\mathbf{B}_{core}(\mathbf{r},t)+\mathbf{B}_{crust}(\mathbf{r})}_{Aperiodic}+\underbrace{\mathbf{B}_{disturbance}(\mathbf{r},t)}_{Periodic+Stochastic} \tag{9}$$

where $\mathbf{B}_{core}$ - the core field generated in the Earth's conducting, fluid outer core (primary geodynamo effect, about 95% $\mathbf{B}_m$); $\mathbf{B}_{crust}$ - the crustal field from the Earth's crust/upper mantle (about 4% $\mathbf{B}_m$); $\mathbf{B}_{disturbance}$ - the combined disturbance field from electrical currents flowing in the upper atmosphere and magnetosphere, which also induce electrical currents in the sea and the ground (secondary geodynamo effect). The $\mathbf{B}_{core}$ and $\mathbf{B}_{crust}$ are quasi-static (they have a secular variation), whereas $B_{disturbance}$ is rapidly time-varying (it has periodic and stochastic contributions).

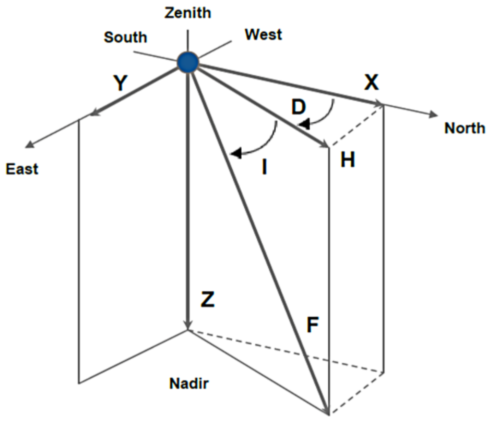

Fig. 9. The elements of the field vector describing the Earth's magnetic field **[15]**

Seven elements are needed to describe the field, generated by a variety of sources, Fig. 9. Table 1 shows the expected range of the magnetic field elements at the Earth's surface.

Components X, Y, Z, F or H, *D*, Z, F are recorded precisely by the ground-based observatories of the Earth's geomagnetism and by low orbit satellites – with an accuracy higher than 1 nT (induction) and 0.001 A/m (intensity), averaging values in a minute-period. Geomagnetic measurements are by two/three orders of magnitude more accurate than MMM measurements currently applied in non destructive testing of elements made of ferromagnetic steel. When the results of the MMM method are analyzed, a simplified model of the Earth is applied and an influence of components B_{crust} and $B_{disturbance}$ is excluded. Nevertheless, these components can't be omitted in structural health monitoring systems (SHM) that are based on high-sensitivity sensors of the magnetic field and the trend analysis.

Table 1. Range of magnetic elements at the Earth's surface (epoch 1.01.2010) **[32].**

Element	Name	Alternative name	Range of the Earth's surface			Positive sense
			Min	Max	Unit	
X	North component	Northerly intensity	-17000	42000	nT	North
Y	East component	Easterly intensity	-18000	17000	nT	East
Z	Down Component	Vertical intensity	6700	61000	nT	Down in the northern Hemisphere
H	Horizontal intensity		0	42000	nT	
F	Total intensity	Total field	22000	67000	nT	
I	Inclination	Dip	-90	90	Degree	Down
D	Declination	Magnetic variation	-180	180	Degree	East clockwise

3.1. A model of the Earth's magnetic field

A very convenient way of representing geomagnetic fields $\mathbf{B}_m$ is to expand the scalar magnetic potential *V* into the spherical harmonic function [30-32]. In geocentric spherical coordinates (longitude λ, latitude φ', radius r) it can be written as the negative spatial gradient of a scalar potential.

$$\mathbf{B_m}\left(l,\phi',r,t\right)=-\nabla V\left(\lambda,\phi',r,t\right)$$
$$V\left(\lambda,\phi',r,t\right)=a\left\{\sum_{n=1}^{N}\sum_{m=0}^{n}\left(g_n^m\left(t\right)\cos\left(m\lambda\right)+h_n^m\left(t\right)\sin\left(m\lambda\right)\right)\left(\frac{a}{r}\right)^{n+1}P_n^m\left(\sin\phi'\right)\right\} \tag{10}$$

where *N* is the degree of the numerical model, *a* = 6371200 m is the geomagnetic reference radius, $g_n^m(t)$ and $h_n^m(t)$ are the time-dependent Gauss coefficients of degree *n* and order *m* describing the Earth's main magnetic field (they are based on measurements made by satellite, airborne, and at the surface). $P_n^m(\mu)$ are the Schmidt semi-normalized associated Legendre functions.

Such a model can be subsequently evaluated at any desired localisation to provide the magnetic field vector, its direction or the anomaly of the total intensity of the field. Verified models of the Earth's magnetism enable obtaining an accurate the reference signal ($\mathbf{B}_{m\_ref} = \mathbf{B}_m \pm 5$ nT) for the MMM expert analysis [29], Fig. 10.

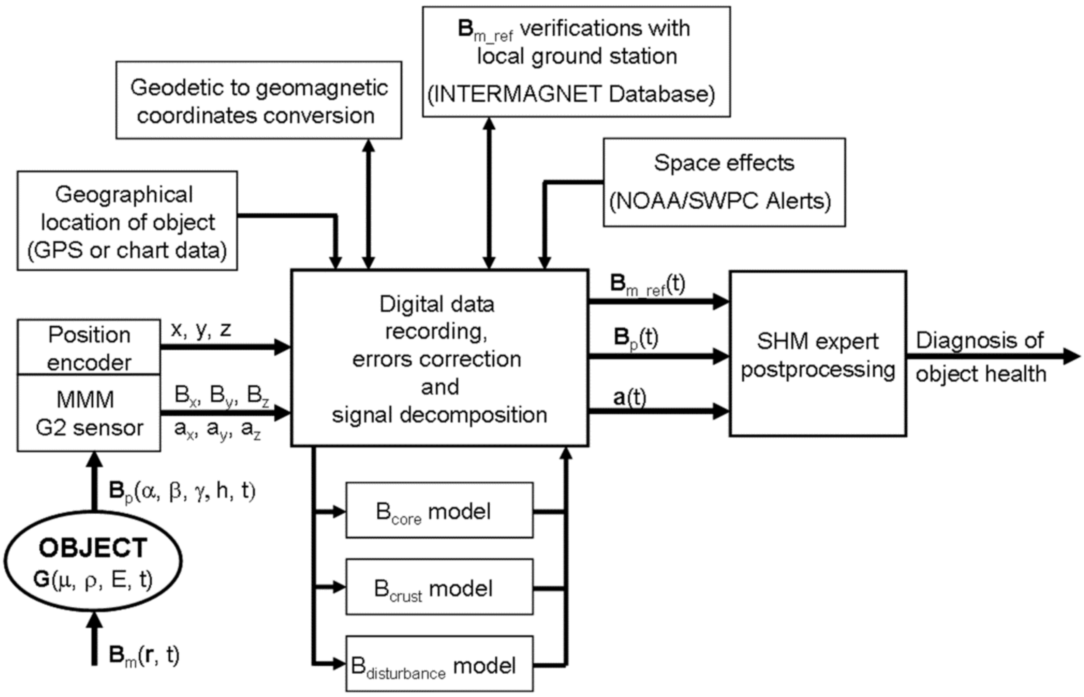

Fig. 10. The SHM expert system based on MMM data (α, β, γ, h – the MMM sensor position in local coordinates relates to the object surface; MMM G2 sensor (MEMS) includes 3 channels of magnetometer (B_x, B_y, B_z) and 3 channels of accelerometer (a_x, a_y, a_z); $\mathbf{B}_{m\_ref}$ – estimator of $\mathbf{B}_m$ near the object surface; a(t) = [$a_x(t)$, $a_y(t)$, $a_z(t)$] - signal of object deformation and vibration

3.2. $\mathbf{B}_{core}$ - verified models

Determination of the expected value for $\mathbf{B}_{core}$ is based on free of charge low degree models, i.e. the International Geomagnetic Reference Field IGRF-11 [34, 35] or the World Magnetic Model WMM-2010 [32, 36]. The source code is in the public domain and not licensed or under copyright.

The data and charts produced from IGRF and WMM models characterize only the long-wavelength portion of the Earth's internal magnetic field (waveband of 2500 km), which is primarily generated in the Earth's fluid core, Fig. 11. The portions of the geomagnetic field generated by the Earth's crust and the upper mantle, and by the ionosphere and the magnetosphere, are largely unrepresented in the $\mathbf{B}_{core}$ models. Consequently, a magnetic sensor may observe spatial and temporal magnetic anomalies (typically of the magnitude 200 nT, but often much larger - up to several thousands of nT) when referenced to the models. In particular, certain local, regional, and temporal magnetic declination anomalies can exceed 10 degrees.

a) b)

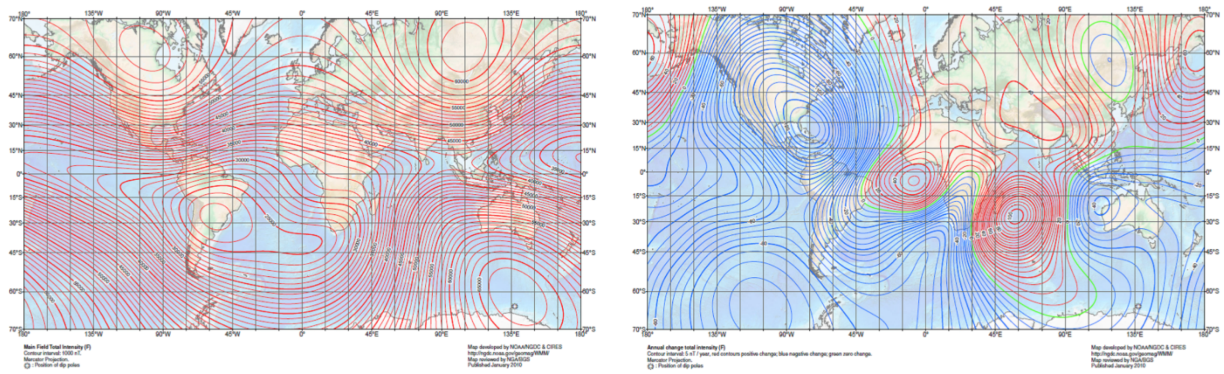

Fig. 11. Result of WMM-2010 model (epoch 2010,0) for: a) total intensity; b) annual change of total intensity [34]

3.3. B_{crust} - verified models

Subtracting the appropriate IGFR or WMM from the observatory spline function (trend) gives the $\mathbf{B}_{crust}$ part of the internal field that is not represented by the $\mathbf{B}_{core}$ models. $\mathbf{B}_{crust}$ has spatial variations on the order of meters to thousands of kilometers and can’t be fully modeled with low degree spherical harmonic models. On land, spatial anomalies are produced by mountain ranges, ore deposits, ground struck by lightning, geological faults [37] and cultural features such as trains, planes, vehicles, railroad tracks, power lines, etc. The corresponding deviations are usually smaller at sea. In ocean areas these anomalies most frequently occur along continental margins, near seamounts, and near ocean ridges, trenches, and fault zones, particularly those of volcanic origin. The rock magnetization resulting in $\mathbf{B}_{crust}$ may be either induced (by the core field) or remnant or a combination of both types.

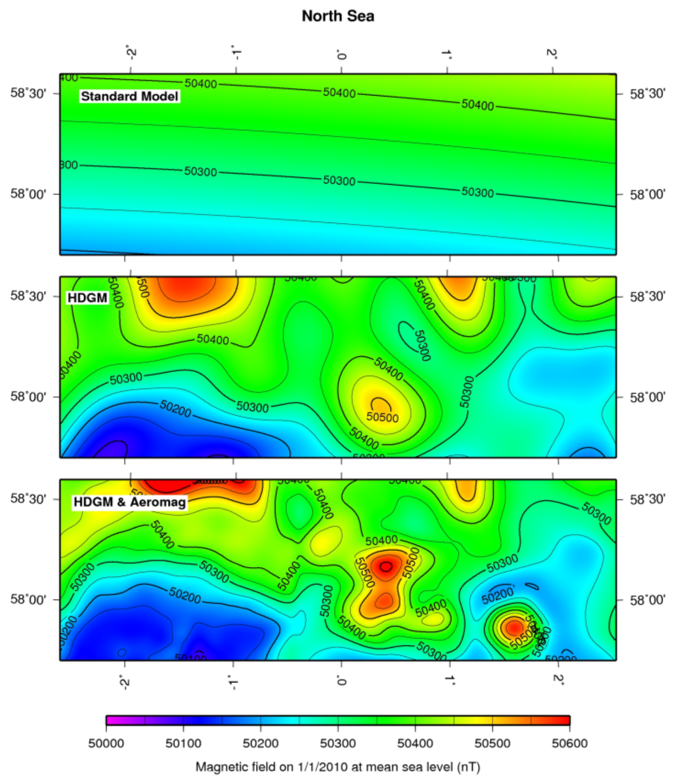

***Fig. 12. Influence degree of numerical model on B_{crust} field component detection (short wave anomalies up to 150 nT is detected by aeromagnetic measurement)* [39]**

A convenient way of representing local magnetic anomaly is to expand the scalar magnetic potential into spherical functions, Fig.12. The free of charge the NGDC-720 and EMM-2010 models [38] provide such an expansion for the crustal field from spherical harmonic degree 16 to 720 (516 736 Gauss coefficients), corresponding to the waveband of 2 500 km to 56 km. The models were compiled from satellite, marine, aeromagnetic and ground magnetic surveys. The degree 720 cut-off corresponds to an angular wavelength of 30 arc minutes, providing a 15 arc minute model resolution. The models are produced at 5-year intervals. To meet the increasing demand for accurate geomagnetic referencing, NGDC produces the High Definition Geomagnetic Model (HDGM) [39], which accounts for long-wavelength crustal magnetic anomalies. The HDGM significantly reduces geomagnetic referencing errors. The HDGM model includes the main field, secular variation and crustal field to degree 720 (similar in properties to the NGDC-720 and EMM-2010 models) but it is updated annually. The HDGM is available for purchase from NGDC.

3.4. The $B_{disturbance}$ component

Of more importance to the MMM expert systems is the $\mathbf{B}_{disturbance}$ component (external and secondary magnetic field) which has periodic and irregular variation, Fig. 13. Knowledge about this component makes it possible to recognize early symptoms of structure defects and continuous damage, and to minimize wrong diagnoses.

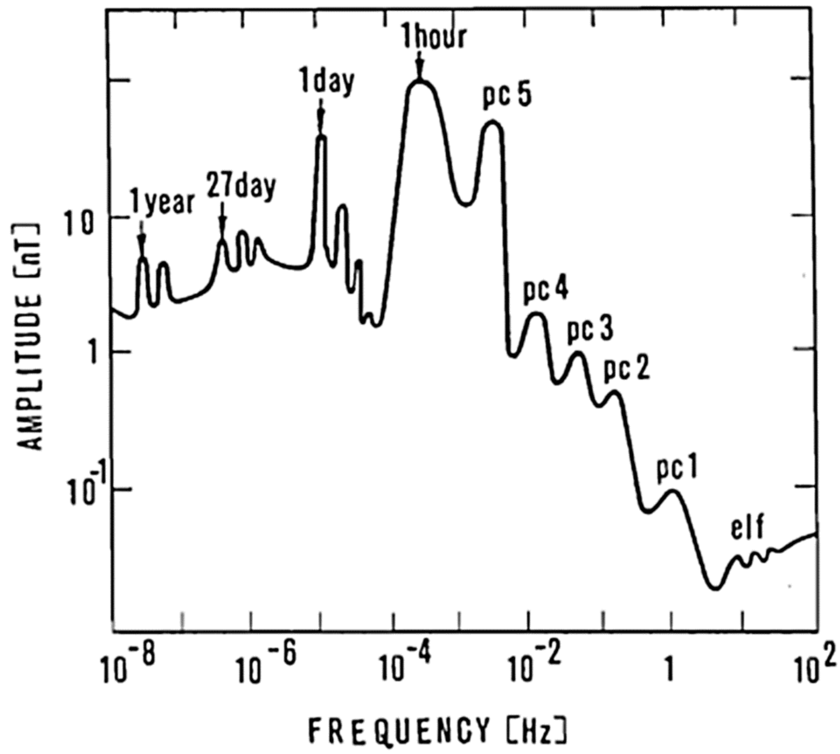

***Fig. 13. Amplitudes of natural variation of the horizontal component H ('pc' - continuous pulsations, 'elf' – extremely low frequency portion of electromagnetic field or Schumann resonance)* [30]**

The regular variations of the magnetic field are related to rotation and/or orbital movements of the Earth, Sun and Moon [30, 33]. They can be divided into four main classes: daily, seasonal, 27-day and 11-year variations. The most prominent is the diurnal variation having a magnitude of the order of 10-100 nT, Fig. 14.

The irregular variations of $\mathbf{B}_{disturbance}$, occurring at a time scale mostly ranging from seconds to hours, are related to the Sun's activity and space magnetic impulse – magnitude variation up to 1000 nT and more during a magnetic storm, Fig. 15. and [40]. On a longer time scale (days to years), the large-scale magnetic field of the external ring current (approximately represented by the D_{st} index) will give perhaps 1000 nT during and after a magnetic storm. Risk of magnetic storm and wrong MMM diagnose are correlated with:

- the sunspot number and scale of the phenomena, Fig. 16 and Table 2;
- interplanetary disturbances from the Sun (solar wind value);

which describe the official planetary K_p index. This index is derived by calculating a weighted average of the K-index from a network of geomagnetic observatories. The K-index is a code that is related to the maximum fluctuations of horizontal components observed on a magnetometer relative to a quiet day, during a three-hour interval, Table 3.

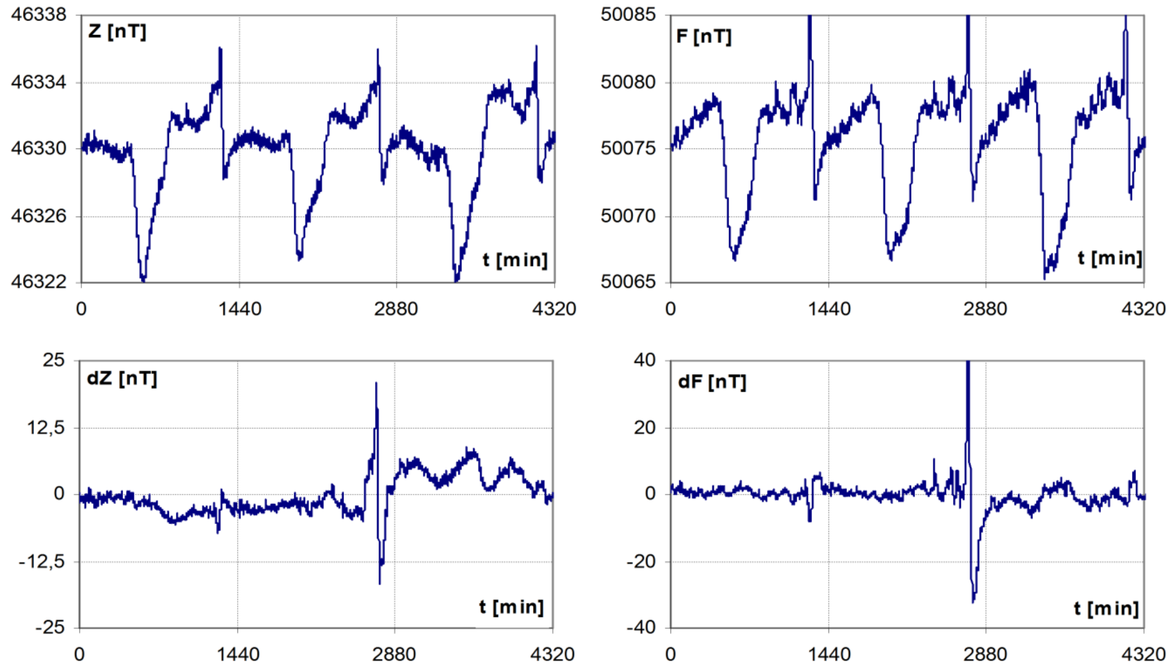

Fig. 14. Detection of regular and stochastic components of $B_{disturbance}$ during 3-day observation (1-minute averaging, midnight at 0, 1440, 2880 and 4320 min UTC, tail current influences on Z and F values close the magnetic midnight, data source: BEL Belsk, Poland* [41]*)

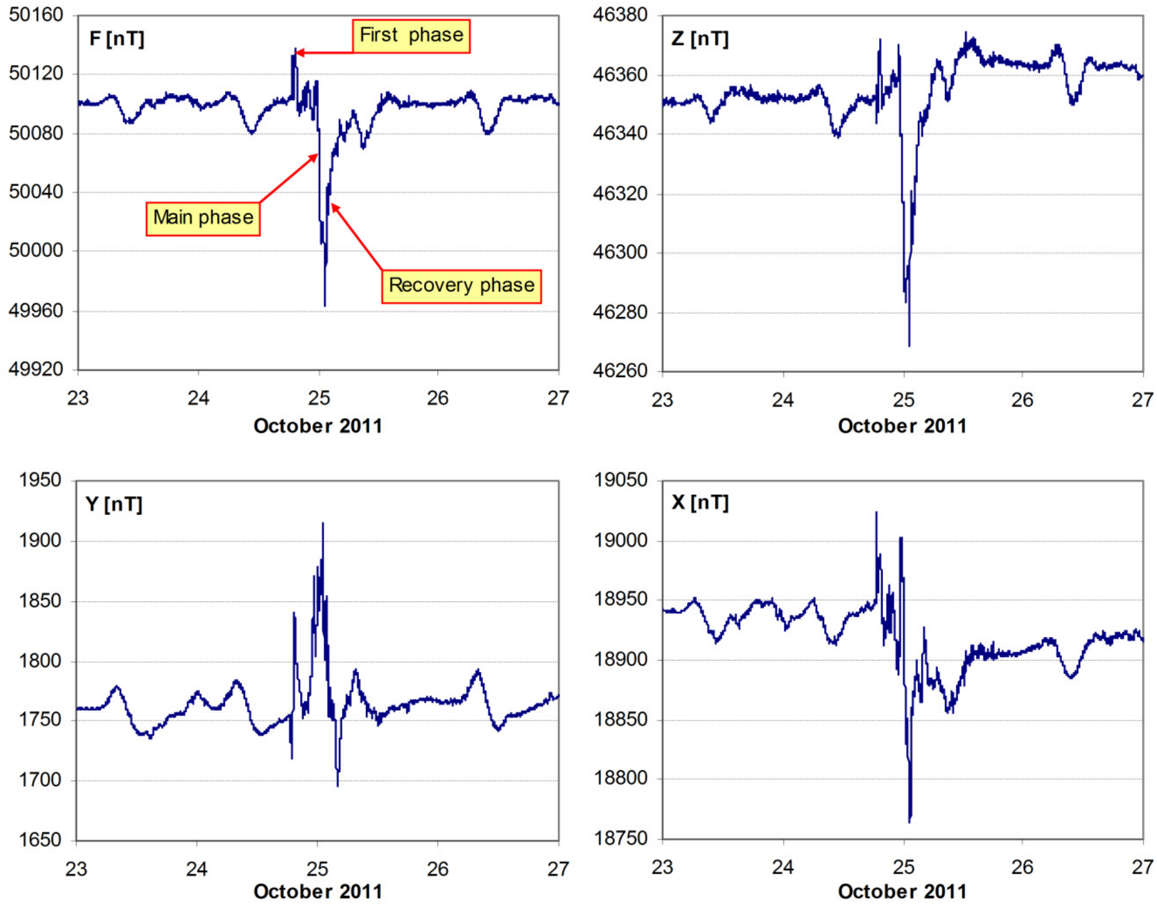

Fig. 15. The influence of space activity (G2 storm detected by GEOS satellites [42]) on the input signal for MMM applications (the geomagnetic field measured by the ground observatory BEL Belsk, Poland* [41]*)

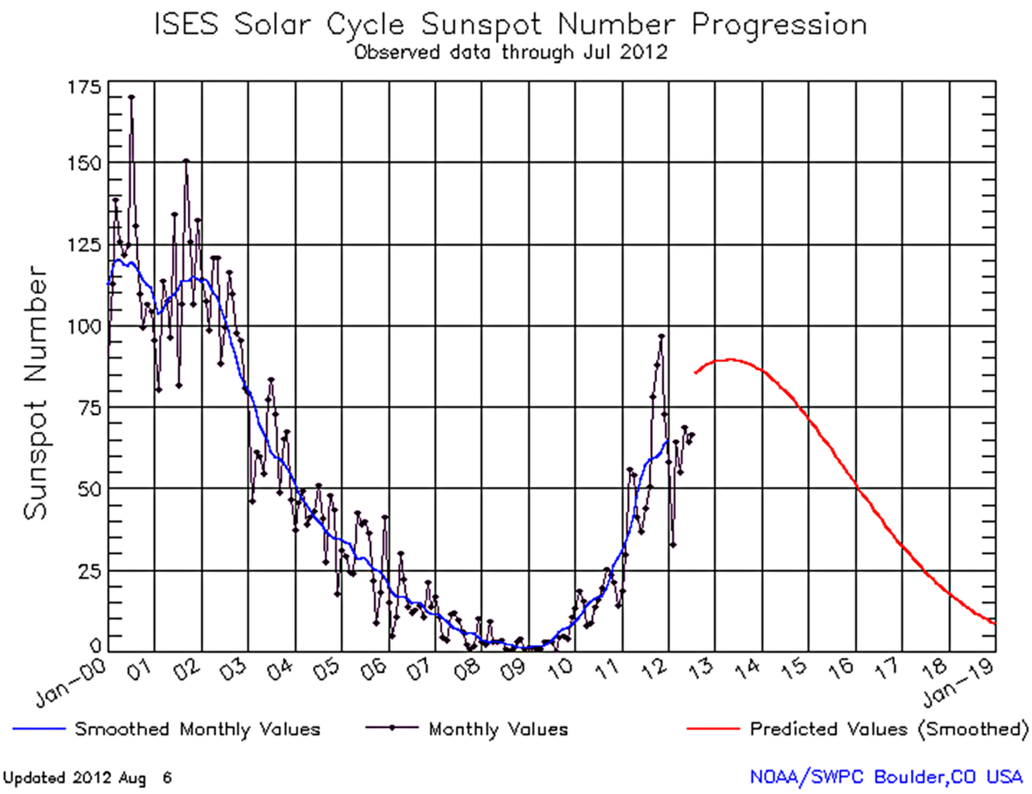

Fig. 16. The Solar Cycle 24 (prediction and the Sun's real activity) **[42]**

Table 2. NOAA space weather scale for geomagnetic storms **[42]**

Category		Physical Measure	Average frequency (1 cycle = 11 years)	Risk level of false diagnose for MMM applications
Scale	Descriptor			
G5	Extreme	$K_p = 9$	4 per cycle (4 day per cycle)	Very high risk above 40° geomagnetic latitude
G4	Severe	$K_p = 8$	100 per cycle (60 days per cycle)	Very high risk above 45° geomagnetic latitude
G3	Strong	$K_p = 7$	200 per cycle (130 days per cycles)	High risk above 50° geomagnetic latitude
G2	Moderate	$K_p = 6$	600 per cycle (360 days per cycle)	Medium risk above 55° geomagnetic latitude
G1	Minor	$K_p = 5$	1700 per cycle (900 day per cycle)	Medium risk above 60° geomagnetic latitude
G0	Below storm	K_p of 0 to 5		Low risk

Table 3. The relation between the K-index and maximum fluctuation of horizontal components observed on a magnetometer **[42]**

K	[nT]	K	[nT]	K	[nT]	K	[nT]	K	[nT]
0	0 – 5	**1**	5 – 10	**2**	10 – 20	**3**	20 – 40	**4**	40 – 70
5	70 – 120	**6**	120 – 200	**7**	200 - 330	**8**	330 – 500	**9**	> 500

The irregular variation $\mathbf{B}_{disturbance}$ can also represent $\mathbf{B}_{crust}$ changes near the monitoring object whose source is a volcano or seismic activity [43-46]. These phenomena represent stress induced magnetization of rock, similar to the MMM symptoms used for monitoring steel objects.

Algorithms based on the Julian calendar and the magnetic local time (MLT) are required in order to perform analyses of the $\mathbf{B}_{disturbance}$ periodical variation. Data from local INTERMAGNET observatory [41, 47] and from the developed analysis algorithm are also used.

In order to identify a stochastic component (the Sun's activity and magnetic impulses from the space) converted satellite-data (NOAA/SWPC alerts [42]) are applied.

4. CONCLUSIONS

The numerical verified models of $\mathbf{B}_{core}$, $\mathbf{B}_{crust}$ and $\mathbf{B}_{disturbance}$ Earth's fields have been proposed to generate high-quality reference signals for the MMM expert systems (for NDT, SHM and PHM applications) and identify new diagnostic symptoms, as well as for the systematic/periodic calibration of the magnetic field sensors, taking the time of the testing and the location of the monitoring object into consideration. Verified models of the Earth's magnetism enable obtaining an accurate reference signal $\mathbf{B}_{m\_ref} = \mathbf{B}_m \pm 5$ nT.

In order to precisely determine the $\mathbf{B}_{disturbance}$ component for monitoring objects of significance located in the Polish territory (applications of SHM and PHM with the use of the MMM method), the following data are anticipated to be used:

- reference data from ground-based observatories,
- correction data (RTK) from the system of ground-based reference observatories ASG EUPOS,
- converted data from SWPC NOAA.

Expected effects of the use of external reliable sources of data in MMM expert systems are as follows:

- an improvement in reliability and resolution of the $\mathbf{B}_{m\_ref}$ reference signal for a randomly chosen location for the monitored object;
- a capability to diagnose and predict regular and irregular geomagnetic phenomena in the vicinity of the monitored object.

ACKNOWLEDGEMENTS

The study has been prepared under the research project "Monitoring of Technical State of Construction and Evaluation of its Lifespan" (MONIT) financially supported by the European Regional Development Fund and the Ministry of Regional Development of Poland in the Innovative Economy Operational Programme (POIG 1.2).

The results presented in this paper rely on data collected at magnetic observatories. We thank the national institutes that support them and INTERMAGNET for promoting high standards of magnetic observatory practice (www.intermagnet.org).

REFERENCES

[1] Birss, R.R. & Faunce, C.A. (1971). Stress-Induced Magnetization in Small Magnetic Fields, *Journal de Physique*, Colloque C I, supplément au n° 2-3, Tome 32, Février-Mars, page C 1 – 686-688.

[2] Altherton, D.L. & Jiles, D.C. (1986): Effects of stress on magnetization, *NDT International*, Vol. 19(1), pp. 15-19.

[3] Robertson, I.M. (1991): *Magneto-Elastic Behaviour of Steels for Naval Applications,* MRL Technical Report, MRL-TR-90-27, *DSTO Materials Research Laboratory*.

[4] Tae-Kyu Lee, Morris J.W., Seungkyun Lee, Jr. & Clarke, J. *Detection of fatigue damage prior to crack initiation with scanning SQUID microscopy*. Review of Progress in Quantitative Nondestructive Evaluation, Vol. 25.

[5] Witoś, M. (2011). *Increasing the durability of turbine engine components through active diagnostics and control*. Research works of AFIT, Issue 29 (in polish).

[6] Vlasov, V.T. & Dubov, A.A. (2004). *Physical bases of the metal magnetic memory method*, ZAO Tisso Publishing House.

[7] Liu Q., Lin J., Chen M., Wang C., Wang G., Zhao F.Z., Geng Y., Zheng Ch. (2008). *A Study of Inspecting the Stress on Downhole Metal Casing in Oilfields with Magnetic Memory Method*, Proc. of 17th World Conference on Nondestructive Testing, 25-28 Oct 2008, Shanghai, China.

[8] Hu B., Chen G., Shen G., Li L., Chen X. (2008). *Study on Magnetic Memory Method (MMM) for Fatigue Evaluation*, Proc. of 17th World Conference on Nondestructive Testing, 25-28 Oct 2008, Shanghai, China.

[9] Zhong L., Li L., Chen X. (2008). *Progress in Nondestructive Evaluation of Stress Concentration with MMM Method*, Proc. of 17th World Conference on Nondestructive Testing, 25-28 Oct 2008, Shanghai, China.

[10] Roskosz, M. (2011). Metal magnetic memory testing of welded joints of ferritic and austenitic steels, *NDT&E International*, Vol. 44, pp. 305-310.
DOI:10.1016/j.ndteint.2011.01.008.

[11] Roskosz M., Rusin A. & Kotowicz J. (2010): The metal magnetic memory method in the diagnostics of power machinery components, *Journal of Achievements in Materials and Manufacturing Engineering*, Vol. 43(1), pp. 362-370.

[12] Viana A., Rouve L-L., Cauffet G. & Coulomb J-L. (2011). *Analytical Model for External Induction Variations of a Ferromagnetic Cylinder Undergoing High Mechanical Stresses in a Low Magnetic Field of Any Orientation*. IEEE Transactions on Magnetics, Vol. 47, No. 5

[13] Dobmann, G. *Physical basics and industrial applications of 3MA – micromagnetic multiparameter microstructure and stress analysis*, Fraunhofer IZFP, Saarbrücken, Germany.

[14] Burrows, C.W. (1916). *Correlation of the magnetic and mechanical properties of steel*, Scientific Papers of the Bureau of Standards, No 272, Government Printing Office, Washington.

[15] Newnham, R. (2005). *Properties of materials. Anisotropy, symmetry, structure*. Oxford University Press.

[16] Fonteyn, K.A. (2010). *Energy-based magneto-mechanical model for electrical steel sheets*. Doctoral Dissertation, Aalto University, TKK Dissertations 234.

[17] Dapino, M.J. (1999). *Nonlinear and hysteretic magnetomechanical model for magnetostrictive transducers*. PhD Dissertation, Iowa State University.

[18] Gallaudet, E.F. (1896). *Relation between length, elasticity and magnetization of iron and nickel wires*. PhD Dissertation, Johns Hopkins University.

[19] Nagaoka H. & Honda K. (1898-1925). *Researches on Magnetostriction*. The Journal of the College of Science, Imperial University of Tokyo, Section 353.

[20] The Journal of the College of Science, Imperial University of Tokyo 1901-1908, Vol. XVI, Article 8-10, 12-14.

[21] Hobbie, Jr. J.R. (1922). Magnetostriction with small magnetizing fields. *Physical Review*, Vol. XIX, No. 5.

[22] Lee, E.W. (1955). Magnetostriction and Magnetomechanical Effects. *Rep. Prog. Phys*., Vol. 18, p. 184 –229.

[23] Tomohiro Yamasaki, Shinji Yamamoto, Masahiko Hirao (1996). Effect of applied stresses on magnetostriction of low carbon steel. *NDT&E International*, Vol. 29(5), pp. 263-268.

[24] Smith C.M., Geo. W. Sherman, Jr. (1914). A study of the magnetic qualities of stressed iron and steel. *Phys. Rev.*, N. S., 4, pp. 267-273.

[25] Sandford, R.L. (1924). Effect of stress on the magnetic properties of steel wire. *Scientific Papers of the Bureau of Standards*, Vol. 19, No 469-497.

[26] Kocańda, S. (1957). Wykrywanie wad metali metodą magnetyczną. PWN Warszawa.

[27] http://www.ndt.net/

[28] http://www.ibgndt.com/

[29] Witoś, M. (2012). The reference signal of geomagnetic field for MMM expert systems. *Key Engineering Materials*, Vol. 518, pp. 384-395. DOI:10.4028/www.scientific.net/KEM.518.384

[30] Jankowski J. & Sucksdorff Ch. (1996). *Guide for magnetic measurement and observatory practice*, IAGA, Warsaw.

[31] Maus S. (2006). *Plane and spherical harmonic representations of the geomagnetic field*, CIRES, University of Colorado, February 16, 2006.

[32] Maus S., Macmillan S., McLean S., Hamilton B., Thomson A., Nair M., Rollins C. (2010). The US/UK World Magnetic Model for 2010-2015*, NOAA Technical Report NESDIS/NGDC*.

[33] Sabaka T.J. *Earth's dynamic magnetic field. The state of the art comprehensive model*. GSFC

[34] http://www.iugg.org/IAGA

[35] http://www.ngdc.noaa.gov/IAGA/vmod

[36] http://www.ngdc.noaa.gov/geomag/WMM/

[37] Pharaoh T. & TESZ colleagues: *Trans-European Suture Zone. Phanerozoic Accretion and the Evolution of Contrasting Continental Lithospheres*. http://www.geofys.uu.se

[38] http://www.ngdc.noaa.gov/geomag/EMM/index.html

[39] http://www.geomag.us/models/HDGM.html

[40] *The largest magnetic storm on record. The "Carrington Event" of August 27th to September 7th 1859, recorded at Greenwich Observatory*, London, British Geological Survey.

[41] http://www.intermagnet.org

[42] http://www.swpc.noaa.gov

[43] Davis P.M., Pierce D.R., McPherron R.L., Dzurisin D., Murray Th., Malcom J.S., Johnston S. & Mueller R. (1984). A volcanomagnetic observation on Mount St. Helens, Washington, *Geophysical Research Letters*, Vol. 11(3), pp 233-236.

[44] Yasunori Nishida, Mitsuru Utsugi, Toru Mogi (2007). Tectonomagnetic study in the eastern part of Hokkaido, NE Japan (II): Magnetic fields related with the 2003 Tokachi-oki earthquake and the 2004 Kushiro-oki earthquake. *Earth Planets Space*, Vol. 59, pp. 1181-1186.

[45] Shu-Kun Hsu, Yi-Ching Yeh, Chung-Liang Lo, Andrew Tien-Shun Lin, and Wen-Bin Doo (2008). Link between Crustal Magnetization and Earthquakes in Taiwan. *Terr. Atmos. Ocean. Sci.*, Vol. 19(5), pp. 445-450, DOI: 10.3319/TAO.2008.19.5.445(T).

[46] Meirav Bass (2010). *Investigation of geodynamic phenomena from high-resolution magnetic measurements*. M.Sc. Thesis to the Department of Geophysics and Planetary Sciences, Tel Aviv University, Jaruselem.

[47] Benoît St-Louis [ed.] (2011). *Intermagnet technical reference manual*, INTERMAGNET c/o British Geological Survey Murchison House, Edinburgh.